Available online at www.sciencedirect.com
ScienceDirect
Acta Materialia 58 (2010) 1994–2003
Acta MATERIALIA
www.elsevier.com/locate/actamat

On the stress-free lattice expansion of porous cordierite

Giovanni Bruno [a,*], Alexander M. Efremov [b], Bjørn Clausen [c], Anatoly M. Balagurov [d], Valeriy N. Simkin [d], Bryan R. Wheaton [e], James E. Webb [e], Donald W. Brown [c]

[a] Corning SAS, CS&S, CETC, F-77210 Avon, France
[b] Corning Inc., Modeling and Simulation, CSC, St Petersburg, 194021, Russia
[c] Los Alamos National Laboratory, LANSCE, Los Alamos, NM 87545, USA
[d] FLNP, JINR, Dubna, 141980, Russia
[e] Corning Inc., CS&S, SP, Corning, NY 14830, USA

Received 13 March 2009; received in revised form 23 November 2009; accepted 24 November 2009
Available online 8 January 2010

Abstract

An extensive investigation of the lattice expansion (up to 1200 °C) of porous synthetic cordierite (obtained by firing a mixture of talc, clay, alumina and silica) was carried out using time-of-flight neutron diffraction at LANSCE, Los Alamos, NM, USA and FNLP, Dubna, Russia. An extruded rod and several powders, with different particle size (dispersity), were studied, with the aim of monitoring the variation of the (lattice) micro-strain as a function of temperature and its influence on the microscopic and macroscopic thermal expansion. Results show a different expansion of the *a*- and *b*-axes of the orthorhombic cell (in the rod above 800 °C). While the finest powder seems to contract more along the *c*-axis, thus hinting at the presence of smaller stress, the integral peak width increases as a function of temperature in the intermediate range (300–700 °C). This could be explained by the integrity factor modeling in terms of micro-cracking. In polycrystalline cordierite, the model implies tension along the *a*- and *b*-axes (positive thermal expansion) accompanied by compression along the *c*-axis (negative thermal expansion) and a stress release upon cooling, via a thermal micro-cracking mechanism. The calculations of the cordierite macroscopic thermal expansion having as input crystal axial expansions assumed to be stress-free allowed us to conclude that even a fine powder (5 μm particle size) cannot be considered completely stress-free. This conclusion is supported by microstructural observations.

Keywords: Micro-strains; Neutron diffraction; Thermal expansion; Integrity factor; Micro-cracking

1. Introduction

Low thermal expansion ceramics are of great interest for diverse applications such as environmental emissions reduction, support for catalytic converters, refractories, cookware and telecommunications [1]. One of the main requirements for their practical use is a high thermal shock resistance [2]. Key factors affecting this resistance, and in general to the reliability of these ceramics, are the coefficient of thermal expansion (CTE), the elastic modulus (E) and the modulus of rupture (MOR) [3]. This class of materials, including cordierite, exhibits the following microstructural and crystallographic features: (1) they are porous (to different degrees); (2) they possess strongly anisotropic single crystal properties, in particular CTE, and generally have low crystal symmetry); (3) they show the phenomenon of micro-cracking; (4) they generally possess morphological and crystallographic texture.

As a typical example, synthetic cordierite obtained by firing a mixture of talc, clay alumina and silica has crystallites with a prismatic shape, and sizes of approximately 1 × 3 μm, with their long axis parallel to the crystal axis *c* of the orthorhombic cell. They typically organize themselves in (roughly spherical) domains of about 10–30 μm size, usually having orientations contained within ±10° (see Ref. [3] and below).

* Corresponding author. Tel.: +33 164 697040; fax: +33 164 697454.
E-mail address: brunog@corning.com (G. Bruno).

1359-6454/$36.00 © 2009 Acta Materialia Inc. Published by Elsevier Ltd. All rights reserved.
doi:10.1016/j.actamat.2009.11.042

Collections of domains form the polycrystal. Due to the thermal expansion mismatch and to the misorientation of the domains, thermal stresses are inevitably generated during firing or cooling from the firing temperature. Eventually, if those stresses exceed a critical value, the domains detach from each other and microcracks appear.

Recently, the link between micro-cracking and its origin—the anisotropy of crystal expansion—was modeled using the concept of the integrity factor [7], applied to different materials.

The lattice expansion has been studied in many systems [8,9]. In particular, the cordierite lattice expansion has been studied by several authors in the 1970s and 1980s [4–6, 10–14]. Among these works, only Mirwald [13] and Milberg and Blair [11] used temperatures up to 1000 °C. Recently, advanced techniques such as synchrotron radiation have been used, but the experimental data is still limited to 800 °C [14]. Some of the main conclusions derived from the previous studies are that the presence of secondary phases and the crystal chemical composition strongly affect the bulk thermal expansion properties [4–6].

Neutron diffraction has established itself as a very reliable technique for in situ measurements of internal strains [15,16]. This technique has several advantages: (1) neutrons uniquely penetrate matter and thus allow bulk investigations, discarding misleading surface effects; (2) unlike laboratory X-rays, the use of a special sample environment is not a limitation, for the same reason as in (1) ; (3) new instrumentation and neutron sources enable short counting times. In particular, the time-of-flight (ToF) technique allows all peaks to be detected in a large *d*-spacing range and therefore allows the use of Rietveld refinement to extract the overall cell parameters and the peak widths, which can be utilized to determine microstructural parameters, such as micro-strains.

Moreover, a decisively important advantage of ToF instruments is that the resolution function is practically constant in a very large *d*-spacing range. This helps to extract microstructural parameters with extremely high precision.

This study seeks to use the significant improvements in diffraction equipment and high-temperature furnaces, to investigate the effect of different levels of micro-strains in a typical synthetic porous polycrystalline ceramic such as cordierite. The lattice expansion for powders of different particle size (dispersity) has therefore been studied and referred to a compact sample which is expected to have the maximum level of micro-cracking and stresses locked into the microstructure. The results have been modeled on the basis of the so-called integrity factor model, introduced in Ref. [7].

2. Experimental methods

2.1. Sample preparation and characterization

A cordierite composition produced at Corning Inc., by extruding and firing a mixture of talc, alumina, clay and silica, has been used for all investigations (for the composition and the firing see Refs. [17,18]). Four kinds of samples have been extracted from a single batch: an extruded rod (diameter 8 mm) and three powder batches ball-milled from the same rod. The powders were sieved to maximum particle sizes of 5, 15 and 1000 μm (measured with standard laser diffraction on a coulter counter, Varian). The nominal porosity of the rod was 48% (determined by mercury porosimetry on an Autopore 9520 Micromeritics).

The X-ray diffraction phase analysis of the material is given in Table 1 (see also Refs. [17,18]). Although typically indialite (or high cordierite) is present, in our case the main component was found to be low cordierite (with orthorhombic crystalline symmetry). The typical resulting microstructure is shown in Fig. 1a. As can be seen, crystallites of typical size $1 \times 1 \times 3$ μm organize themselves into domains of approximate size about 10–20 μm. Microcracks creating during cooling from the firing temperature (>1400 °C) are also visible (see the white arrows). In spite of the large domain size, the microstructure stays polycrystalline-like even in the powder particles, Fig. 1b, which still consist of a collection of small (misoriented) crystallites.

Neutron diffraction texture analysis, fully reported in Ref. [19], showed a low level of texture (1.2× random), with the *c*-axis oriented along the extrusion direction.

Classical dilatometry was also carried out on an extruded cellular sample (a square prism of $5 \times 5 \times 50$ mm size) of exactly the same composition, using a Netzsch DL 402C single pushrod dilatometer. A ramp of 10 °C min^{-1} on both heating and cooling was used. The macroscopic expansion is displayed in Fig. 2. It must be noted that some small hysteresis occurs, due to the well-known phenomenon of retarded microcrack opening upon cooling.

2.2. Time-of-flight neutron diffraction

In situ high-temperature neutron diffraction measurements were completed at the Lujan Center at LANSCE, Los Alamos National Laboratory, NM, USA, using the engineering diffractometer SMARTS (spectrometer for materials research at temperature and stress) [20], and at the IBR-2 Reactor of the Frank Laboratory for Neutron Physics at the JINR, Dubna, Russia, using the powder diffractometer HRFD (high-resolution Fourier diffractometer) [21].

SMARTS is a second-generation engineering diffraction instrument, purposely designed and built to measure internal strains at non-ambient conditions. In the present work

Table 1
The phase analysis of the material studied.

Phase	Phase analysis (%)
Low cordierite	95+
Spinel	3–5
Alumina	0
Mullite	0
Glass	1–5

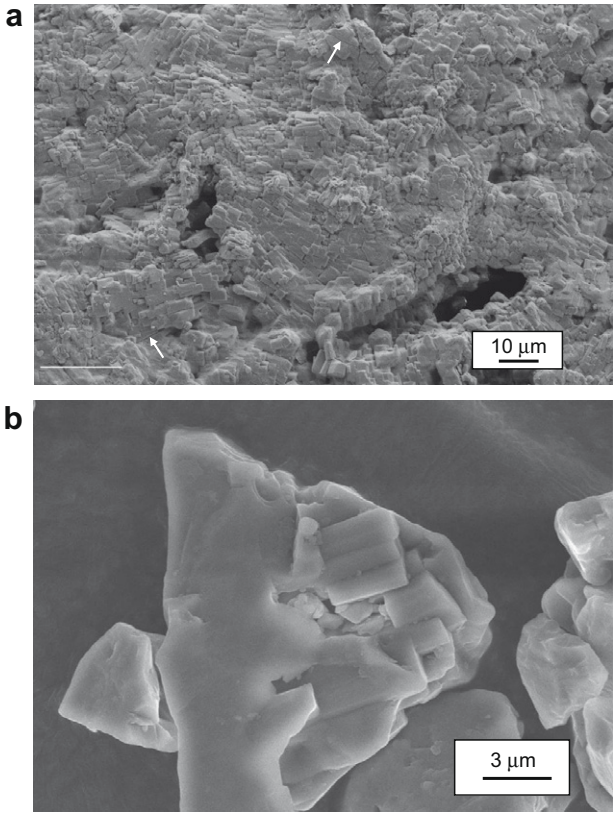

Fig. 1. (a) The typical microstructure of porous cordierite, as taken on the rod (the white arrows indicate microcracks, the white line the extrusion axis). (b) A micrograph of the 15 μm powder. Crystallites are visible in the particles. Courtesy Cedric Le Goff, Corning SAS, CETC-Avon, France.

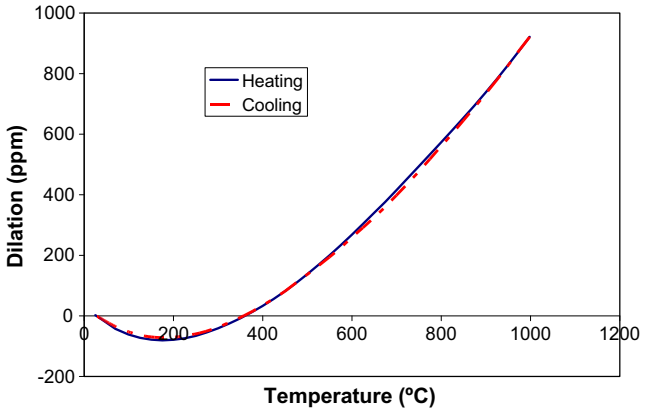

Fig. 2. The macroscopic dilation curve of the synthetic cordierite material of the present work. Heating and cooling branches are represented.

we employed the high-temperature vacuum furnace manufactured by Materials Research Furnaces. It allows in situ measurements up to 1800 °C in a stand-alone configuration, or up to 1500 °C when used in combination with the Instron load frame.

Fig. 3 shows the furnace used for the experiments on SMARTS. While usually the gauge volume, i.e. the volume probed by the neutron beam, is defined by the use of two radial collimators, one for each detector, in our case no collimator was used, since the gauge volume is naturally

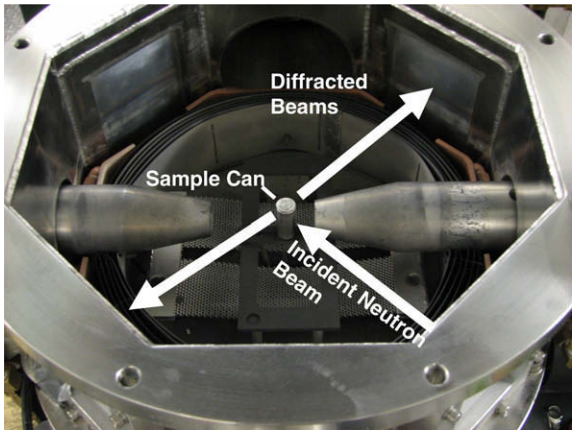

Fig. 3. The high-temperature furnace on SMARTS, LANSCE, Los Alamos, NM, USA. The detectors are located towards the top right and the bottom left corners. The neutron path into the sample and the furnace is shown for clarity. The diameter of the vessel is about 35 cm.

defined by the sample size and the encumbrance of the furnace does not allow mounting of the collimators.

In the case of SMARTS, neutron diffraction data were collected as a function of temperature from room temperature (RT) to 1200 °C. Measurements were made every 25 °C and cycles were recorded (heating and cooling). Since the ToF technique is used at LANSCE, and a large neutron wavelength spectrum is used as a probe, full pattern Rietveld refinement was used to determine the lattice parameters for the orthorhombic (low) cordierite phase, using the program GSAS [22]. In particular, on SMARTS, the available d-spacing range is contained between 0.05 and 0.38 nm. The typical counting time for a whole pattern was about 20 min. Powders were canned in niobium sample holders, while the rod was mounted vertically on a boron nitride holder in the middle of the hot zone.

HRFD (High-resolution Fourier diffractometer) is the ToF correlation neutron spectrometer utilizing the fast Fourier chopper for modulation of the neutron beam intensity and the reverse time-of-flight (RToF) method for registration of scattered neutrons [21,23]. This improves the resolution of the final spectrum to about $\delta d/d \sim 10^{-3}$. The diffractometer benefits of three detector banks, two in backscattering ($2\theta \sim 150°$) and one at 90° (usually used for stress analysis). The in-house built furnace mounted on HRFD is shown in Fig. 4. It is capable of reaching 900 °C, but due to the long counting times (~4 h) needed in our work, the maximum temperature has been limited to 800 °C. In the case of RToF spectra, a special Rietveld refinement program has to be used, to cope with negative counts, and therefore the program MRIAWIN [24] has been used.

3. Results and considerations

3.1. Time-of-flight neutron diffraction data

As mentioned above, the lattice parameters a, b, c of the orthorhombic low cordierite phase have been

Fig. 4. The high-temperature furnace on HRFD, FNLP, Dubna, Russia. The height of the furnace section is about 10 cm.

determined by a Rietveld refinement of the diffraction patterns at each temperature for each sample. They are shown in Fig. 5.

The values of the lattice parameters were averaged between detector banks 1 and 2 (collecting signals along perpendicular scattering vectors), since they should yield the same results, because of symmetry reasons (as mentioned, the rod was mounted vertically). Indeed, the relative shift between the two detector banks has proven to be very small.

Although no physical reason holds to give a larger weight to the room temperature (RT) lattice parameter values (e.g. the signal-to-noise ratio is not best at RT), the calculation of the dilation (strain) was done assuming the measured value at RT to be the reference (see Fig. 6), i.e. we defined the dilation as $[d(T) - d(\mathrm{RT})]/d(\mathrm{RT})$, where d is the lattice spacing. This procedure only introduces a possible shift, which does not influence the relative variation of the strain as a function of temperature.

With the reference lattice parameters, the crystal strains in all samples and all crystal directions could be calculated and are reported in Fig. 6.

Fig. 5 shows an essential equivalence among the lattice parameters of all samples in the a and b directions: it is possible that the 5 μm powder possesses a lower b-lattice parameter (as well as some degree of hysteresis) and the 1000 μm powder has a higher a-lattice parameter at low temperatures (below 600 °C). From both Figs. 5 and 6 we can notice that in all samples the c-axis contracts on heating and expands on cooling at intermediate temperatures ($T < 600$ °C). On heating, a distinctive behavior can be noticed for the c-axis: the lattice parameter change between RT and 1200 °C is highest in the 5 μm powder, while the total range of variation of the dilation is highest in the rod (the dilation parabola looks more concave than for the other samples).

Moreover, while for the powder samples (1000 and 5 μm particle size) the basal axes a and b have different lattice expansion (Fig. 6b and c) throughout the whole temperature range, for the rod they differ only above 800 °C

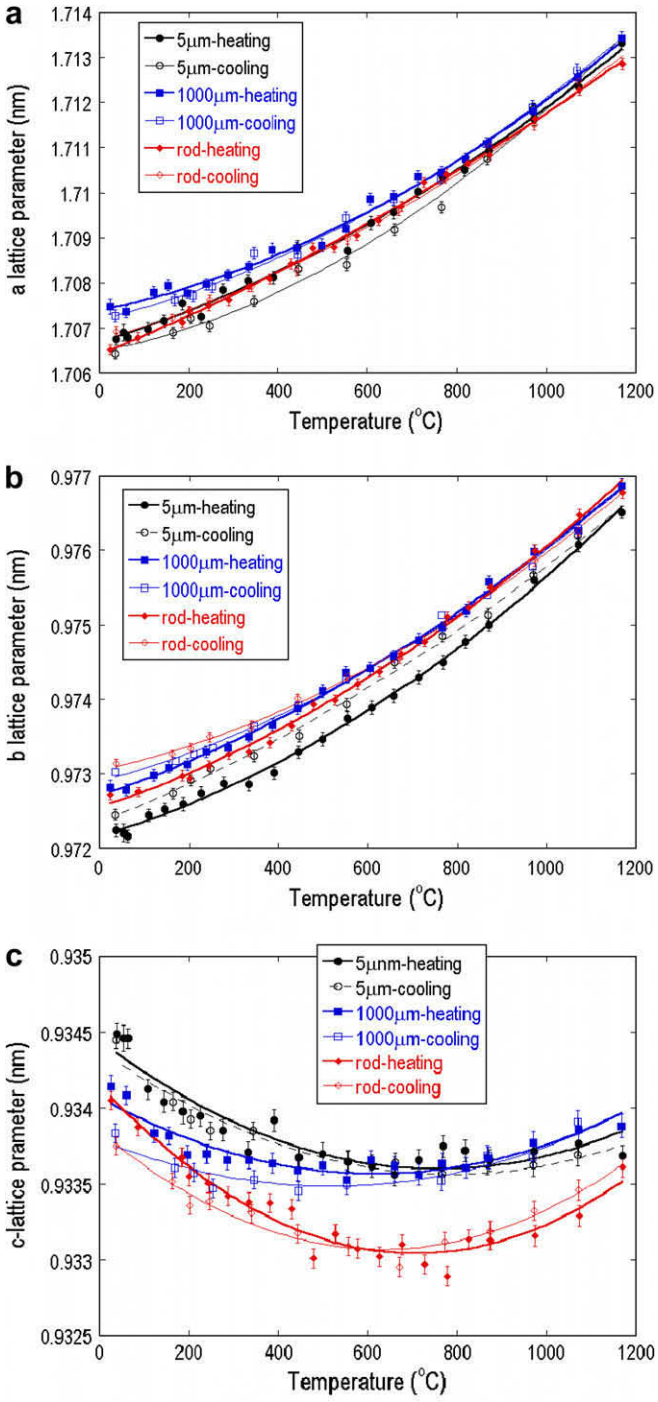

Fig. 5. The lattice evolution in the three crystal directions for the studied cordierite material: compact rod, 1000 μm and 5 μm particle size powders. The heating and cooling data are shown by full and hollow symbols, respectively.

(Fig. 6a). Interestingly enough, the heating and cooling cycles show hysteresis for all cases, possibly with the exception of the 5 μm powder c-axis and the 1000 μm powder a-axis. The difference between heating and cooling must be interpreted in terms of micro-cracking: possibly, the rod and the 1000 μm powder c-axis cracks and therefore relaxes stresses, while the a- and b-axes in the 5 μm powder

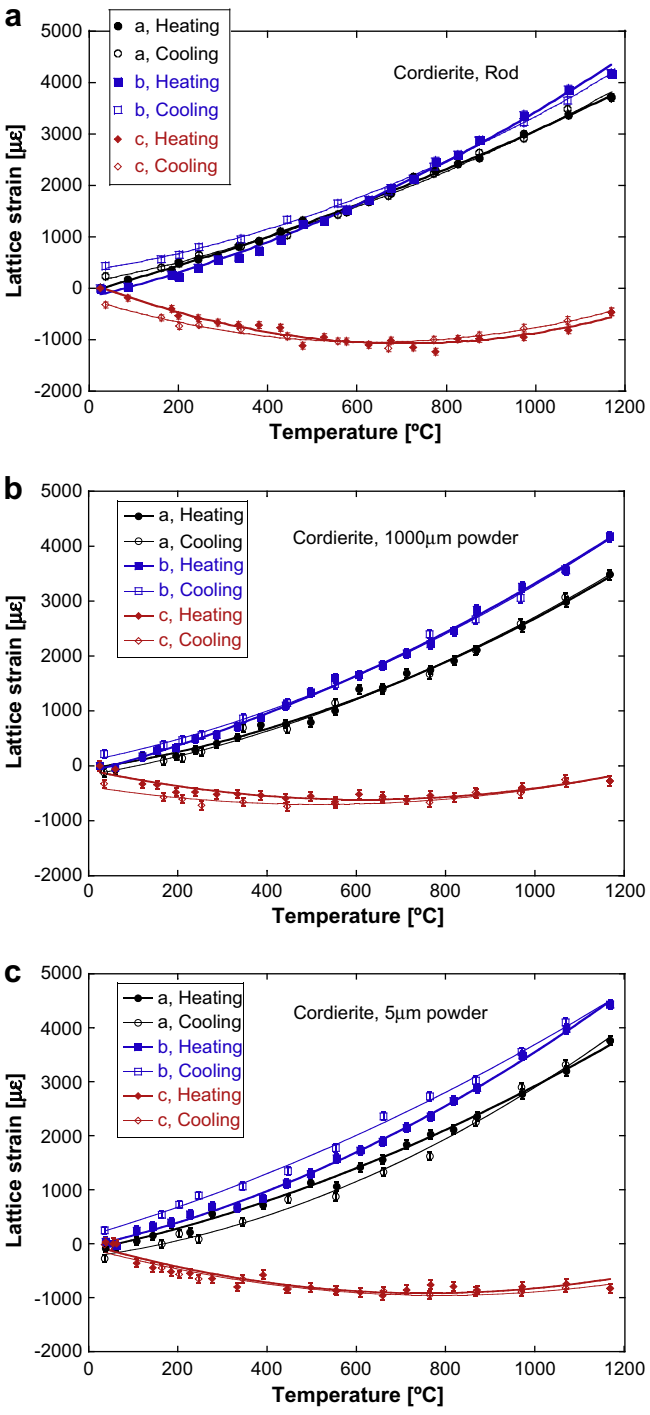

Fig. 6. The dilation in the three crystal directions for the studied cordierite: compact rod (a), 1000 μm (b) and 5 μm (c) particle size powders. The heating and cooling ramps are shown (thick and thin lines plus full and hollow symbols, respectively).

seem to strain in opposite directions upon cooling. This would imply a phenomenon of load transfer from *a* to *b*: the tensile strain in the *b*-axis could be generated by excess micro-cracking along *a*, which in turn relaxes towards compression (see also the modeling section below).

An alternative view of the results shown in Figs. 5 and 6 can be shown in Table 2, where the CTE α along all crystal directions are shown for all the samples. We define the CTE as

$$\alpha = \frac{d(T) - d(\mathrm{RT})}{d(\mathrm{RT})} \cdot \frac{1}{T - \mathrm{RT}}$$

While the *a*-axis seems to expand more in the rod and in the 5 μm powder than in the 1000 powder, i.e. it holds

$$\alpha_{a_{rod}}^{25\text{–}1200} \approx \alpha_{a_{5\ \mu m}}^{25\text{–}1200} > \alpha_{a_{1000\ \mu m}}^{25\text{–}1200}$$

the *b*-axis seems to expand more in the 5 μm powder than in the rod:

$$\alpha_{b_{5\ \mu m}}^{25\text{–}1200} > \alpha_{b_{1000\ \mu m}}^{25\text{–}1200} \approx \alpha_{b_{rod}}^{25\text{–}1200}$$

and the *c*-axis to contracts more in the 5 μm powder than in the rod:

$$\alpha_{c_{1000\ \mu m}}^{25\text{–}1200} \geqslant \alpha_{c_{rod}}^{25\text{–}1200} > \alpha_{c_{5\ \mu m}}^{25\text{–}1200}$$

as well as

$$\alpha_{c_{1000\ \mu m}}^{25\text{–}750} > \alpha_{c_{5\ \mu m}}^{25\text{–}750} \geqslant \alpha_{c_{rod}}^{25\text{–}750}$$

From the Rietveld fit, the squared peak width (w^2) dependence on the squared *d*-spacing (or the squared wavelength) was extracted. In fact, according to the GSAS manual [22], the peak integral width *w* is modeled as a function of *d* using some coefficients w_i, $i = 0,2$:

$$w^2(d) = w_0^2 + w_1^2 d^2 + w_2^2 d^4 \qquad (1)$$

The $w_2{}^2$ term depends on the crystallite size as $w_2 \propto 1/D$; therefore, the term in d^4 can often be considered negligible, if the crystals are not nano-sized. Moreover, for nearly all spectra, the fit yielded $w_2^2 \sim 0$ and $w_0^2 \sim 0$ when all three parameters were let free. Therefore only w_1 was taken into account to represent the integral width. According to classical diffraction theory (see e.g. the overview in Ref. [25]), w_1 represents a combination of the isotropic contribution of strain broadening and the instrumental resolution. However, a plot of the behavior of w_1 as a function of *T* (Fig. 7) can be a good indicator of the evolution of the intra-granular stresses [25]. It is indeed interesting that the peak width parameter w_1 for the 5 μm powder has a different behavior from heating to cooling, while the other two samples do not show any hysteresis. This confirms that the rod and the 1000 μm powder behave similarly. Moreover, the integral peak width of the 5 μm powder has a bell-shaped form, while for the other two samples it is flatter, and slightly decreases with temperature.

3.2. Reverse time-of-flight neutron diffraction data

Fig. 8 shows the neutron diffraction data acquired at FLNP, Dubna, Russia. There, the same rod and the 15 μm powder were measured. Quite remarkably, the rod and powder data coincide, in spite of the very small error bar. This holds basically for all directions, except maybe for the *c*-axis, where the powder seems to contract more. However, little data is available on the powder (up to

Table 2
The CTE between 25 and 1200 °C in the three crystal directions, as measured at Los Alamos for the compact rod, the 1000 μm and the 5 μm particle size powders, all in ppm °C^{-1}.

Sample	α_a (25–1200 °C)	α_b (25–1200 °C)	α_c (25–1200 °C)
Rod	3.16 ± 0.06	3.56 ± 0.07	-0.39 ± 0.06
1000 μm Powder	2.96 ± 0.07	3.56 ± 0.08	-0.23 ± 0.07
5 μm Powder	3.20 ± 0.07	3.77 ± 0.07	-0.71 ± 0.07

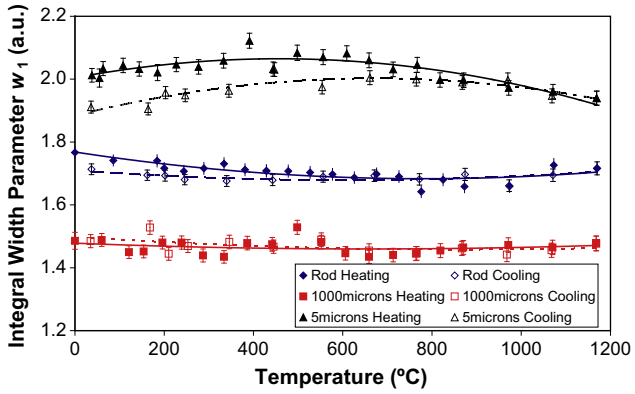

Fig. 7. The integral width parameter w_1 for the three samples measured at Los Alamos. The heating and cooling branches are shown, fitted by thick and thin lines, respectively. Values are displaced for different datasets for the sake of clarity.

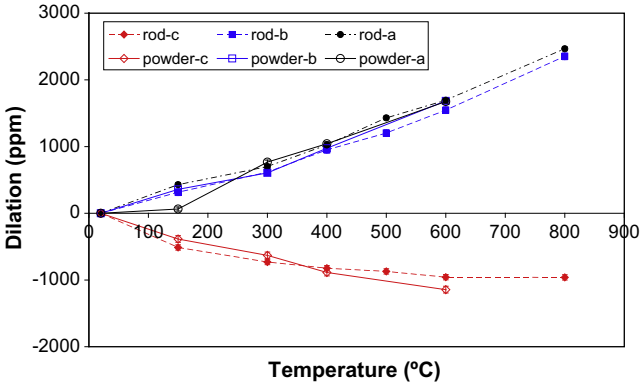

Fig. 8. The neutron data collected at Dubna, Russia, on the 15 μm powder and on the compact rod. Lines are guides for eye. The error bars are contained in the symbols.

600 °C). The *a*- and *b*-directions also coincide, as it happens in the Los Alamos data up to 800 °C.

3.3. Comparison between present and literature results

The overall agreement between the two neutron sources is very good. For the rod, at Los Alamos *b* dilates more than *a*, but only above 800 °C. Otherwise, the two curves perfectly match those found at Dubna below 800 °C, where the *a*- and *b*-expansion coincide (Fig. 9a). The *c*-direction data also seem to basically coincide in the range of superposition. For the powders (Fig. 9b), we compared the 15 μm at Dubna to the 5 μm at Los Alamos: the *b*-expansions at Dubna and Los

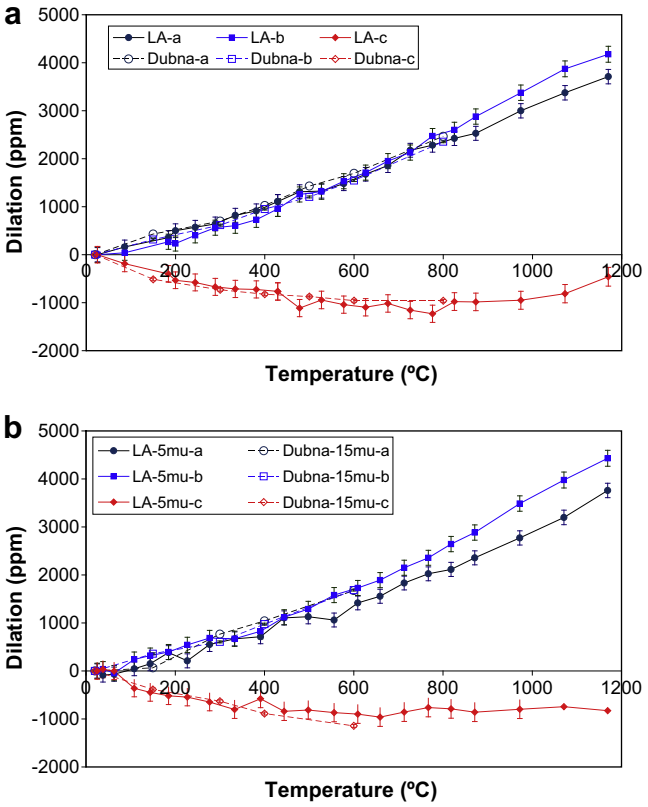

Fig. 9. The comparison of the measured expansion at Los Alamos and Dubna: (a) the rod data, (b) the powder data plus the average of the $(a + b)$ directions at Los Alamos. Lines are guides for the eye.

Alamos coincide, while the *a*-expansion seems to differ above 500 °C. The different dispersity could explain this quantitative mismatch, especially because the *c*-axis also seems to slightly differ. Both facts call for a different amount of micro-strains locked in the structure.

In Fig. 10 data from previous works from Milberg and Blair [11], Hochella et al. [4], and Fischer et al. [10] as reported in Evans et al. [6], as well as Lee and Pentecost [26] are superposed to the Los Alamos and Dubna rod

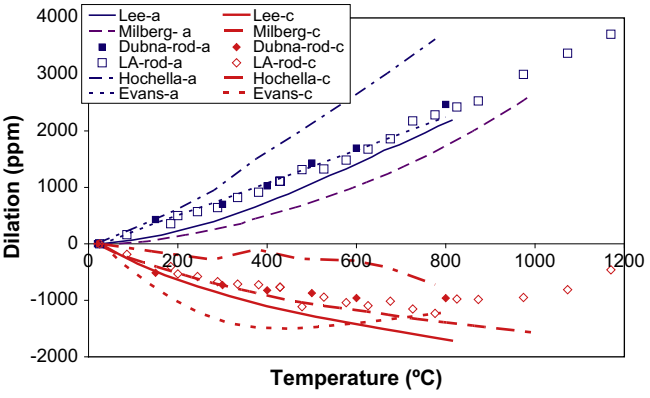

Fig. 10. A comparison between the present lattice expansion data and previous works from Hochella, Evans, Lee and Milberg. Only some of the experimental data of this work were used, and no error bars are displayed for the sake of clarity.

data. It can be seen that the agreement is very good and the present data (both neutron sources) agree particularly well with the work of Milberg and Blair and with the data from Fischer et al. for the *a*-axis. Some discrepancies can be seen with the data collected by Hochella et al. [4]; however, in that case, the *a*-axis data show higher expansion and the *c*-axis less contraction. This could be due to the fact that the material used by Hochella contains higher stresses and/or its chemical composition (Mg-rich in that case) constrains the lattice to a larger extent. As mentioned in the introduction, different cordierite solid solutions have proven to yield different thermal expansions [4–6].

4. Modeling

From the considerations of the previous section, it turns out that it is very important to investigate the evolution of grain strains (also called micro-strains) as a function of temperature, during both heating and cooling. This is particularly true when one wants to assess the thermal shock resistance of brittle materials [2]. As mentioned above, usually, cooling from the firing temperature creates intergranular cracks (or thermal micro-cracking) in these materials. Due to the grain anisotropy the axes of high CTE (*a* and *b*) contract on cooling more than the lower CTE axis (*c*) and eventually disconnect from the solid domain, so that contribution of the low CTE axis to the bulk (macroscopic) dilation increases. Crack opening and closure change the mechanical and thermal behavior of these solids and the concept of integrity function has been introduced by Efremov [7] to quantify the influence of intergranular cracking on the CTE of polycrystalline materials with anisotropic properties. This model basically expands the well-known Turner formula [27] and enables the evaluation of the degree of micro-cracking directly from bulk CTE curves of single phase polycrystalline material such as cordierite, as measured by conventional macroscopic dilatometry, for example.

The model [7] defines the macroscopic thermal expansion ε as a function of the lattice stress-free thermal expansion (ε_i), some crystal elastic coefficients (E_i), the *i*-axis texture and volume fraction (V_i) contribution, so that the macroscopic expansion is given by:

$$\varepsilon = \frac{\sum \varepsilon_i V_i E_i \omega_i}{\sum V_i E_i \omega_i} \tag{2}$$

ω_i is the mentioned integrity factor, describing the variation of the *i*-axis lattice contribution to the bulk properties due to the amount of thermal micro-cracking. It varies from 1 (intact state) to 0 (fully microcracked state). By definition the equations

$$\sum V_i = 1 \quad \text{and} \quad 0 \leqslant \omega_i \leqslant 1 \tag{3}$$

hold. The summation is carried over all crystal directions. It can be easily extended to other phases, possibly anisotropic. One can see that the open porosity does not influence thermal expansion as far as $E_{pores} = 0$. The expression of the thermal strain in the range from a reference temperature T_r to a generic temperature T in terms of the instantaneous (differential) CTE $\alpha(T)$ is given by

$$\varepsilon(T_r, T) = \int_{T_r}^{T} \alpha(T) dT \tag{4}$$

We note that all the strains in Eq. (2) are assumed to be evaluated as referred to the same reference temperature T_r. The arbitrary choice of T_r does not undermine the conclusions we draw regarding the lattice and macroscopic thermal expansion. However, the value of T_r does influence the value of grain stresses since it defines the onset of stress development. For this reasons, any conclusion about the stress state will be kept qualitative.

For a single-phase material such as cordierite we can roughly assume the crystal strains along *a* and *b* are the same and the elastic coefficients are the same for all three axes (see also Ref. [28]). Consequently, the evaluation of the integrity factor in the *a*- and *b*-axes from the crystal stress-free data and the macroscopic dilation data is given by (Eq. (2)):

$$\omega_a = \frac{-V_c}{1 - V_c} \cdot \frac{\varepsilon_c - \varepsilon}{\varepsilon_a - \varepsilon} \tag{5}$$

Taking the experimental lattice data from the previous section as stress-free lattice expansions, we can calculate the macroscopic dilation curve for ideally intact, i.e. non-micro-cracked, cordierite materials (called IC in the following). Then, we can compare them to the macroscopic experimental dilation taken upon cooling (Fig. 2).

To achieve this goal, for the sake of simplicity we first performed a polynomial fit of the lattice and macroscopic dilation data (second- and fourth-order polynomial, respectively) and used the obtained coefficients in the calculations, Eq. (2) (collected in Tables 3 and 4).

The macroscopic expansion (upon cooling) of an ideally intact cordierite was then calculated from Eq. (5), using the following conditions:

- assuming $\omega_i = 1$ for all *i* (intact material),
- taking $V_c = 0.46$ (derived from the macroscopic dilation curve derivative at 1200 °C),
- assuming $T_r = 1200$ °C.

Each of the lattice dataset has been taken as a reference in order to test its suitability to represent a stress-free state of the material. In this way, different curves have been obtained, indicated in Fig. 11 as IC with the corresponding stress-free dataset. The integrity factor for the crystal directions *a* and *b*, using the different lattice data as stress-free, is shown in Fig. 12.

One can observe a mismatch among all simulated curves as well as between those and the experimental data. The latter mismatch is due to micro-cracking: the measured macroscopic dilation does contain the contribution of micro-cracking, which is deliberately neglected in the

Table 3
Coefficients of lattice parameter (Å) and cell volume data parabolic fit $Y = c0 + c1 * T + c2 * T^2$, where T is temperature (in °C).

	Sample	$c0$	$c1$	$c2$	R^2	N, points
a (nm)	5 μm	1.7069	2.52×10^{-6}	1.88×10^{-9}	0.988	21
	15 μm	1.7071	3.99×10^{-6}	2.06×10^{-9}	0.974	5
	1000 μm	1.7063	3.09×10^{-6}	1.74×10^{-9}	0.994	21
	Rod	1.7058	4.66×10^{-6}	1.06×10^{-9}	0.997	22
b (nm)	5 μm	0.9721	2.61×10^{-6}	1.28×10^{-9}	0.995	21
	15 μm	0.9734	1.62×10^{-6}	1.85×10^{-9}	0.994	5
	1000 μm	0.9722	3.05×10^{-6}	8.21×10^{-10}	0.998	21
	Rod	0.9721	3.40×10^{-6}	6.70×10^{-10}	0.997	22
c (nm)	5 μm	0.9348	-2.51×10^{-6}	1.37×10^{-9}	0.979	21
	15 μm	0.9354	-2.65×10^{-6}	1.33×10^{-9}	0.995	5
	1000 μm	0.9341	-2.31×10^{-6}	1.39×10^{-9}	0.961	21
	Rod	0.9342	-3.13×10^{-6}	2.22×10^{-9}	0.935	22
Volume (nm^3)	5 μm	1.551	2.27×10^{-6}	6.03×10^{-9}	0.993	21
	15 μm	1.554	1.81×10^{-6}	7.03×10^{-9}	0.990	5
	1000 μm	1.550	3.82×10^{-6}	5.22×10^{-9}	0.997	21
	Rod	1.549	4.43×10^{-6}	5.74×10^{-9}	0.998	22

Table 4
Coefficients of microscopic dilation fourth-order polynomial fit $Y = c0 + c1 * T + c2 * T^2 + c3 * T^3 + c4 * T^4$, where T is temperature (in °C).

Cellular sample	$c0$	$c1$	$c2$	$c3$	$c4$	R^2	N
Bulk	1.54×10^{-5}	-1.24×10^{-5}	4.28×10^{-9}	-3.38×10^{-12}	1.25×10^{-15}	0.9999	54

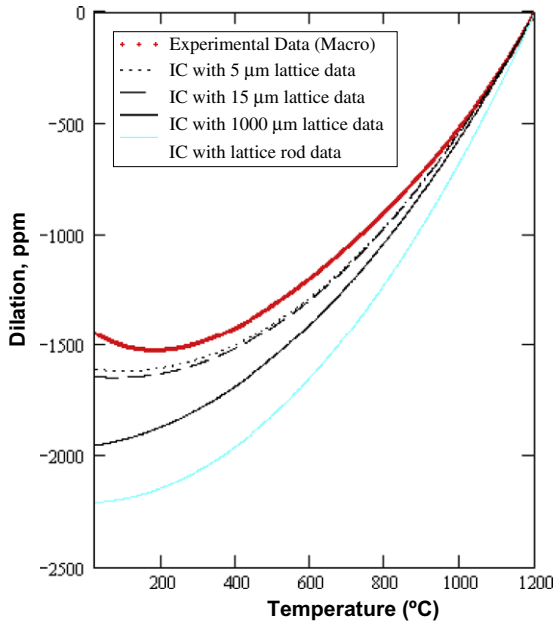

Fig. 11. Macroscopic dilation of the investigated cordierite material (bold line, cooling branch), see Fig. 2, compared with other dilation curves calculated for an ideal (microcrack-free) intact cordierite (IC) using the corresponding lattice data.

simulated curves. In fact, Fig. 11 shows that the experiment and the simulations are close at high temperatures and deviate at lower temperatures: expectedly, there is no micro-cracking at high temperature but a decrease of the integrity factor occurs on cooling (Fig. 12).

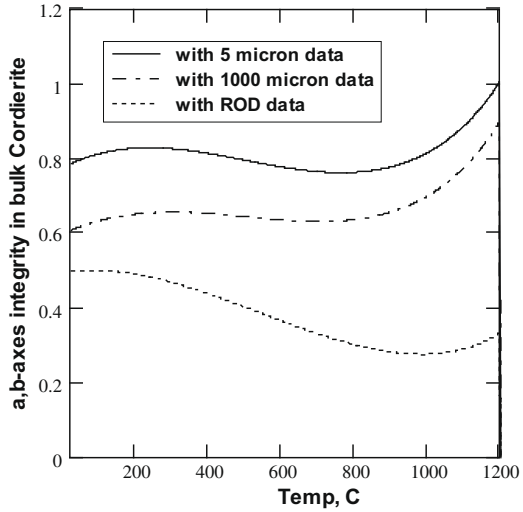

Fig. 12. The integrity factor calculated with Eq. (5), using the input of the different lattice datasets.

5. Discussion

Looking at Fig. 11, we see that the 15 and 5 μm powder lattice data yield similar macroscopic expansion curves, which lie slightly below the measured dilation. On the other hand, the 1000 μm powder and rod lattice data yield very different calculated dilations. Moreover, Table 2 and Fig. 7 show that the 5 μm powder has the highest difference between the a- (or b-) and c-expansion. This means that the stress state in the finest powder is the most relaxed, and the c-axis is truly contracting.

Both facts imply that the 15 and 5 μm powders are good candidates as reference materials, while the 1000 μm powder and the rod are not at all suitable as stress-free materials. In fact, lattice data should correspond to the same material properties, since the crystal composition, crystallite size, etc., are the same for all samples. What yields to different calculated dilations is then the amount of residual micro-stresses carried by each sample. Possibly, defects induced by the stresses themselves and by sample preparation (e.g. grinding) could also play a role. Those factors are able to strongly influence the deviation of the measured lattice data from the intrinsic stress-free lattice parameter values and explain why the simulated data mismatch the experimental dilation curve (Fig. 11).

Furthermore, following the model set forth above, we could calculate the average lattice stress σ_i in each crystal direction i of a polycrystalline material ($i = a, b, c$) by the simple relationship

$$\sigma_i = (\varepsilon - \varepsilon_i) \cdot E_i \cdot \omega_i \tag{6}$$

E_i are the elastic coefficients, proportional to the elastic constants that can be extracted from Toohill et al. [28]. Upon inserting the stress balance equation $\sum \sigma_i V_i = 0$ [27] in Eq. (6) we obtain again Eq. (2).

Eq. (6) shows that for cordierite the principal stress in the a- and b-directions are tensile and that in the c-direction is compressive. The calculation of the temperature-dependent stresses using Eq. (6) and the lattice data as stress-free parameters would yield to the paradox that stresses in the rod are smaller than those in the powders. This contradiction again points out that the rod lattice data are the furthest from the stress-free state and they therefore lead to a gross underestimation of the internal micro-stress.

It is, however, not possible, from the present results, to state that the 5 μm particle size powder is a stress-free material. In fact, several experimental evidences and calculation results point to the fact that even 15 or the 5 μm particles possess some strain inhomogeneity.

1. The integrity factor of the 5 μm powder, extracted from Eq. (2) and shown in Fig. 12, tells us that some microcrack development occurs upon cooling at temperatures below 1000 °C. This is an indicator that some microstress relaxes.
2. The microstructure of the 15 μm powder (Fig. 1b) is a collection of small crystallites and shows all characteristics of a polycrystalline aggregate, analogous to bulk materials. Therefore, the thermal expansion mismatch between the crystal axes of different grains would play a similar role to bulk materials in the onset of stress.
3. The integral peak width of the 5 μm powder is larger than that of the 1000 μm powder and of the rod in the temperature range between 900 °C and RT (see Fig. 7). As mentioned before, this cannot be explained by a domain size effect, which would take place only if the domain size is $D \leqslant 150$ nm, while we have much larger crystallite sizes. Rather, the results of Fig. 7 imply that the micro-strain level in this powder is still detectable. This could be related to a higher level of damage of the crystal structure in the fine powders than in coarse powder and in the rod.

One would expect the lattice to be stress-free in two extreme cases: (1) at very high temperature, say close to the firing temperature, and (2) at very low temperature, when micro-cracking releases all the stresses. In between, stressed non-cracked grains coexist with relaxed cracked grains. The coexistence of the two states of stress effectively increases the width of the diffraction peak and this explains the maximum of the integral width at intermediate temperatures for the 5 μm sample.

6. Conclusions

In this work the lattice expansion of cordierite has been measured by ToF and by reverse ToF neutron diffraction along the three crystal axes of low cordierite (orthorhombic) unit cell. Four samples were chosen: three powders, with different mean particle size (5, 15 and 1000 μm) plus a compact rod. All samples show different expansions along a and b crystal axes, at high temperature, but have equivalent a- and b-expansion behavior below 800 °C. The contraction of the c-axis is very well reproduced at the two neutron sources. Some quantitative (but small) discrepancies are present for the powder samples in all directions: in particular, when comparing the 5 and 15 μm powders measured at Los Alamos and Dubna, respectively, the a- and c-axes seem not to match perfectly. This is certainly an indication that different particle sizes carry different internal micro-strains. The c-axis contraction is more pronounced in the 5 μm powder and smaller in the rod and the 1000 μm powder, consistent with an increasing amount of constraints (i.e. stress) in the latter.

With the lattice data at hand, modeling of the macroscopic dilation of the correspondent intact (non-microcracked) material could be done and of the so-called integrity factor model was applied to all samples. This allowed the observation of the onset of micro-cracking and calculation of the grain stresses. While the latter indirectly shows that the compact rod is more constrained than the powders, especially in the temperature range from 1000 to 200 °C, the integrity factor also shows that the 5 μm powder cannot be considered as a stress-free reference. These theoretical results are well confirmed by the microstructure of the powder and by the behavior of the peak width as a function of temperature: the 5 μm powder shows a bell-shaped integral width as a function of temperature, indicating an onset of micro-strains at high temperature and a relaxation at low temperatures.

Acknowledgments

The authors would like to thank Dr Gregory Merkel (Corning Inc., Corning, NY, USA) for insightful discussions and dilation data. Cedric Le Goff (Corning

SAS-CETC, Avon, France) provided the SEM micrographs (Fig. 1). We acknowledge beamtime at the Lujan Neutron Scattering Center at LANSCE, funded by the US Department of Energy's Office of Basic Energy Sciences. Los Alamos National Laboratory is operated by Los Alamos National Security LLC under DOE contract DE-AC52-06NA25396. We also acknowledge beamtime at the IBR2 Reactor of the Frank Laboratory of Neutron Physics in Dubna, Russia.

References

[1] Van Setten BAA, Makkee M, Moulijn JA. Catal Rev 2001;43:489.
[2] Lu TJ, Fleck NA. Acta Mater 1998;46:4755.
[3] van Roermund HLM, Konert RJ. Phys Chem Miner 1990;17:52.
[4] Hochella M, Brown G, Ross F, Gibbs G. Am Miner 1979;64:337.
[5] Ikawa H, Ushimaru Y, Urabe K, Udagawa S. Sci Ceram 1987;14:234.
[6] Evans D, Fischer G, Geiger J, Martin F. J Am Ceram Soc 1980;63:629.
[7] Efremov AM. Philos Mag 2006;86:5431.
[8] Buessem WR, Thielke NR, Sarakauskas RV. Ceram Age 1952;60:38.
[9] Gillery FH, Bush EA. J Am Ceram Soc 1959;42:175.
[10] Fischer G, Evans D, Geiger J. Crystal lattice thermal expansion of cordierite, abstract B-18 in crystallographic association program and abstracts series 2, vol. 2; 1974. p. 214.
[11] Milberg ME, Blair HD. J Am Ceram Soc 1977;60:372.
[12] Predecki P, Hass J, Faber Jr J, Hitterman RL. J Am Ceram Soc 1987;70:175.
[13] Mirwald PW. Phys Chem Miner 1981;7:268.
[14] Seki H, Miyachi I, Okada T, Yasukawa K, Nishibori E, Kubota Y, et al. Crystal structure analysis of the cordierite ceramics by X-Ray diffraction method using synchrotron radiation, Spring-8 User Exp Rep, vol. 7; 2001A. p 37.
[15] Holden TM, Root JH, Tennant DC, Hosbons RR, Holt RA, Mahin KW, et al. Physica B 1992;180 & 181:1014.
[16] <http://neutron.neutron-eu.net/> or <http://neutron.neutron-eu.net/n_ess>.
[17] Murtagh MJ, Sherwood DL, Socha L. Development of a diesel particulate filter composition and its effect on thermal durability and filtration performance. SAE technical paper 940235; 1994
[18] Merkel GA, Murtagh MJ. Fabrication of low thermal expansion, high porosity cordierite body. Patent EP 0 545 008 A1; 1993
[19] Bruno G, Vogel S. J Am Ceram Soc 2008;91:2646.
[20] Bourke MAM, Dunand DC, Ustundag E. Appl Phys A 2002;74:S1707.
[21] Aksenov VL, Balagurov AM, Simkin VG, Bulkin AP, Kudrjashev VA, Trounov VA, et al. J Neut Res 1997;5:181.
[22] Larson AC, Von Dreele RB. General structure analysis system (GSAS) LANL report LAUR; 2004. p. 86
[23] Hiismäki P, Junttila J, Piirto A. Nucl Inst Meth 1975;126:435.
[24] Zlokazov VB, Chernyshev VV. J Appl Cryst 1992;25:447.
[25] Genzel Ch In Hauk V, editor. Structural and residual stress analysis by non-destructive methods. Amsterdam: Elsevier; 1997. p. 435.
[26] Lee JD, Pentecost JL. J Am Ceram Soc 1976;59:183.
[27] Turner PS. J Res Natl Bur Stand 1946;37:239.
[28] Toohill K, Siegesmund S, Bass JD. Phys Chem Miner 1999;26:333.